Guided ion beam and theoretical studies of the reaction of Ag^+ with CS_2: Gas-phase thermochemistry of AgS^+ and $AgCS^+$ and insight into spin-forbidden reactions

P. B. Armentrout[1,a] and Ilona Kretzschmar[2]
[1]*Department of Chemistry, University of Utah, 314 S. 1400 E. Rm 2020, Salt Lake City, Utah 84112, USA*
[2]*Department of Chemical Engineering, The City College of New York, New York, New York 10031, USA*

(Received 21 October 2009; accepted 13 December 2009; published online 12 January 2010)

The gas-phase reactivity of the atomic transition metal cation, Ag^+, with CS_2 is investigated using guided-ion beam mass spectrometry. Endothermic reactions forming AgS^+ and $AgCS^+$ are observed but are quite inefficient. This observation is largely attributed to the stability of the closed shell $Ag^+(^1S, 4d^{10})$ ground state, but is also influenced by the fact that the reactions producing ground state AgS^+ and $AgCS^+$ products are both spin forbidden. Analysis of the kinetic energy dependence of the cross sections for formation of these two products yields the 0 K bond energies of $D_0(Ag^+—S)=1.40\pm0.12$ eV and $D_0(Ag^+—CS)=1.98\pm0.14$ eV. Quantum chemical calculations are used to investigate the electronic structure of the two product ions as well as the potential energy surfaces for reaction. The primary mechanism involves oxidative addition of a CS bond to the metal cation followed by simple Ag—S or Ag—CS bond cleavage. Crossing points between the singlet and triplet surfaces are located near the transition states for bond activation. Comparison with analogous work on other late second-row transition metal cations indicates that the location of the crossing points bears directly on the efficiency of these spin-forbidden processes. © *2010 American Institute of Physics*. [doi:10.1063/1.3285837]

I. INTRODUCTION

Most second-row transition-metal sulfides find utility as industrial catalysts, where hydrotreating catalysis is of particular interest.[1,2] Silver sulfide, however, is better known for its role during sulfur sensitization in silver-halide photography where the formation of silver sulfide centers with substitutional sulfide ions allows the trapping of photoelectrons leading to an enhanced latent image formation.[3] Silver sulfide is also used as a barrier film in conductance switches of new-generation, nonvolatile solid-state memory devices owing to its mixed ionic conduction properties.[4–6] In addition, silver sulfide has been used both as a polycrystalline membrane by itself or as an active component of a plastic membrane in ion-selective electrode applications.[7] An application of silver sulfide relevant to catalysis is the use of Ag^+-exchanged zeolites for the removal of sulfur compounds from natural gas by formation of stable silver sulfide within the zeolite.[8] Interestingly, Ag^+-exchanged zeolites are also used to synthesize small silver sulfide particles. The smallest particles reported to be formed inside the zeolite pores are the Ag_2S molecule and Ag_4S_2 cluster both of which have temperature-dependent photoluminescent properties in the visible and are useful materials for thermometry.[9]

The introduction of silver ions through medication or silver exposure can lead to generalized argyria,[10] a condition in humans where silver-sulfide deposits in the skin cause a bluish appearance. The postulated mechanism for silver sulfide formation is that Ag^+ reacts with cysteine, which is subsequently destroyed photolytically by UV exposure. Next, Ag^+ is precipitated by nascent SH followed by formation of Ag_2S. The ability of silver and silver ions to bind thiol groups is also employed in the formation of self-assembled monolayers by thiolate molecules on silver surfaces.[11]

While the thermodynamics of the Ag/S system has not been explored experimentally, Arita used experimental sulfur vapor pressure and silver electromotive force data to predict the thermodynamic properties of silver sulfide (α, β, and γ Ag_2S) above 379 K.[12] In previous work, we investigated the gas-phase thermodynamic properties of the sulfides of first-row[13–21] and several early second-row[21,22] transition metal cations, as well as reviewed the periodic trends in this information.[23] In the present study, we investigate the gas-phase thermodynamic properties of cationic silver sulfide (AgS^+), which augments parallel studies of ruthenium, rhodium, and palladium.[24–26] The bonding in AgS^+ is particularly interesting, because the ground state silver ion has a closed 4d shell and empty 5s orbital (^1S). This Ag^+ electron configuration leads to a situation where all ligands, both monovalent CS and bivalent S, are forced to bind via dative rather than covalent interactions in contrast with the situation found with the open 4d shell metal cations, M^+=Ru^+, Rh^+, and Pd^+. The reactions of atomic silver cations with carbon disulfide, CS_2, have previously been studied at room temperature in a high pressure of He by Bohme and co-workers,[27] who observed only $Ag^+(CS_2)$ adduct formation. In the present work, the reaction of Ag^+ with CS_2 is

[a]Electronic mail: armentrout@chem.utah.edu.

studied under single collision conditions using guided-ion beam mass spectrometric techniques. Reactions (1) and (2) are both observed as endothermic processes and their dependence on kinetic energy is measured.

$$Ag^+ + CS_2 \rightarrow AgS^+ + CS, \quad (1)$$

$$\rightarrow AgCS^+ + S. \quad (2)$$

An analysis of the kinetic energy dependence permits the endothermicities of reactions (1) and (2) to be measured and then converted to 0 K bond dissociation energies, $D_0(Ag^+—S)$ and $D_0(Ag^+—CS)$. Quantum-chemical methods are employed to complement the thermodynamic data with information on electronic ground and low-lying excited states, bond lengths, and vibrational frequencies of AgS^+ and $AgCS^+$. Further, the potential energy surface for reaction of both the singlet and triplet spin states is examined and the mechanism for reaction determined. Comparison with companion studies[24–26] elucidates a key factor in the efficiency of these spin-forbidden reactions. Thus, our work presents another case of a reaction involving two potential energy surfaces, which are known to be important in the efficiency of chemical transformations.[28–31]

II. EXPERIMENTAL AND COMPUTATIONAL METHODS

A. Experimental approach

Detailed descriptions of the guided-ion beam apparatus used in this study and the experimental procedures are given elsewhere.[32–34] Briefly, Ar^+ ions created in a dc discharge source[29] are accelerated toward a silver cathode thereby sputtering off Ag^+ ions. The metal ions drift in a meter-long flow tube operated with a 9:1 mixture of helium and argon at a pressure of ~90 Pa. The ions undergo $\sim 10^5$ collisions with the buffer gas before exiting the flow tube, and therefore are expected to equilibrate to room temperature.[35,36] Because helium and argon do not always effectively quench excited states of atomic transition-metal ions,[37] oxygen at ca. 0.27 Pa is introduced about 25 cm downstream from the discharge. Operation at these pressures allows the ions to undergo 10^2–10^3 collisions with O_2 molecules in the flow tube, which is sufficient to remove excited states of the Ag^+ metal ions under study, as shown previously.[35,38,39] This effect is also demonstrated in the present system, as shown below.

Following extraction from the source, the ions are accelerated and focused into a magnetic sector, mass-selected, decelerated to a desired kinetic energy, and focused into an octopole ion guide.[32,40] This device guides the ions through a static gas cell kept at a low pressure (0.01–0.03 Pa) of the reactant gas. It is verified that all product cross sections reported here result from single ion-molecule collisions by examining the pressure dependence of the product intensities. After exiting the gas cell, product and remaining reactant ions drift to the end of the octopole where they are directed into a quadrupole mass filter for mass analysis and then detected. Conversion of the raw ion intensities into reaction cross sections and the conversion from the laboratory (lab) to center-of-mass (CM) energy scale are treated as described previously.[32] Retarding potential measurements are used to determine the distribution and absolute zero of the ion kinetic energy. The accuracy of the absolute cross sections is estimated to be ±20%. The beams have Gaussian kinetic energy distributions with average full widths at half maximum of ca. 0.25 eV in the laboratory frame. The uncertainty of the absolute energy scale is ±0.05 eV (lab).

B. Data analysis

Quantitative analysis of the energy dependence of these cross sections is achieved using Eq. (3) and methods outlined elsewhere.[41–45]

$$\sigma(E) = \sigma_0 \Sigma g_i (E + E_i - E_0)^n / E^m. \quad (3)$$

In Eq. (3), E is the relative kinetic energy of the reactants, E_0 is the threshold for reaction at 0 K, σ_0 is a scaling parameter, and n and m are fitting parameters describing the energy dependence. The summation is over the rovibrational states of the reactants having energies E_i and populations g_i ($\Sigma g_i = 1$) with molecular parameters for CS_2 taken from B3LYP/Def2TZVPP calculations performed here for consistency. (Vibrational frequencies agree with experiment[46] within 3% and the rotational constants are the same.)

In addition to modeling the reaction product cross sections independently using Eq. (3), we also examine competition between the two reaction channels by using a statistical approach that has been described in detail elsewhere,[47,48] Eq. (4).

$$\sigma_j(E) = (n\sigma_{0,j}/E^m) \sum g_i \int_{E_{0,j}-E_i}^{E} [k_j(E^*)/k_{tot}(E^*)] \times [1 - e^{k_{tot}(E^*)\tau}](E - \varepsilon)^{n-1} d(\varepsilon). \quad (4)$$

Here $\sigma_{0,j}$ is a scaling parameter for channel j that is energy independent, $E_{0,j}$ represents the CID threshold energy for channel j at 0 K, ε is the energy available from reactant translation, and τ is the experimental time for dissociation, 5×10^{-4} s. E^* is the internal energy of the energized molecule (EM), i.e., $E^* = \varepsilon + E_i$. The term $k_j(E^*)$ is the unimolecular rate constant for dissociation of the EM to channel j. The rate constants $k_j(E^*)$ and $k_{tot}(E^*)$ are defined by Rice–Ramsperger–Kassel–Marcus[49–51] theory in Eq. (5),

$$k_{tot}(E^*) = \sum k_j(E^*) = \sum d_j N^{\dagger}_{j,vr}(E^* - E_{0\,j})/h\rho_{vr}(E^*), \quad (5)$$

where d_j is the reaction degeneracy for channel j (defined by the ratio of symmetry numbers),[49] h is Planck's constant, $N^{\dagger}_{j,vr}(E^* - E_{0,j})$ is the sum of rovibrational states of the transition state (TS) at an energy $E^* - E_{0,j}$ for channel j, and $\rho_{vr}(E^*)$ is the density of rovibrational states of the EM at the available energy, E^*. TSs for both reaction channels as well as a return to reactants are treated as loose TSs at the phase space limit (PSL),[47] in which case molecular parameters for the EM and TSs are taken from the quantum chemical calculations described below. Note that this treatment locates the loose TS at the top of the centrifugal barrier associated with the separated products, such that ion-molecule capture theory is explicitly followed in a variational approach.[47] In these models, the adiabatic two-dimensional rotational energy is treated using a statistical distribution with explicit

TABLE I. Bond lengths, vibrational frequencies, and state splittings for AgS^- (geometry optimizations and frequency calculations performed at the B3LYP/Def2TZVPP, CCD/Def2TZVPP (bold), and CCSD(T)/Def2TZVPP (italics) levels of theory).

Species	State	r (Å)	ν (cm^{-1})	E_{rel} (eV)[a]	
				B3LYP	CCSD(T)
AgS^-	$^3\Sigma^-$	2.392. **2.487**. *2.434*	237. **211**	0.000	0.000
	$^3\Pi$	2.429	189	0.975	0.943
	$^1\Sigma^-$	2.319	285	1.561	1.458

[a]Relative single point energies calculated at the indicated level of theory using Def2TZVPP basis sets and B3LYP/Def2TZVPP geometries and corrected for zero point energies.

summation over the possible values of the rotational quantum number, as described in detail elsewhere.[47]

Before comparison with the data, Eqs. (3) and (4) are convoluted over the translational energy distributions of both reactants. This determination of the reaction thresholds involves explicit consideration of the distributions of vibrational, rotational, and translational energies of both reactants. Because all sources of reactant energy are considered, the thermochemistry obtained corresponds to 0 K values in all cases.

C. Theoretical approach

We perform calculations using the GAUSSIAN 03 suite of programs[52] with the B3LYP hybrid density functional method[53,54] and Def2TZVPP basis sets, which are balanced basis sets of triple zeta valence quality, with contracted basis functions of [5s3p2d1f] for C, [5s5p3d1f] for S, and [6s4p3d2f1g] for Ag.[55,56] The Def2TZVPP basis set for Ag uses a small core (28 electron) effective core potential developed by Andrae *et al.*[57] These basis sets were obtained from the EMSL basis set library.[58,59] In addition, to provide more accurate thermodynamic information, we also calculate single point energies of Ag^+, S, CS, CS_2, AgS^+, and $AgCS^+$ at the CCSD(T)/Def2TZVPP level of theory[60,61] using B3LYP/Def2TZVPP geometries and zero point energy corrections. This CCSD(T)/Def2TZVPP//B3LYP/Def2TZVPP level of theory is also used to examine the potential energy surfaces for the reactions. In all cases reported below, the single point energies cited include zero point energy corrections using unscaled B3LYP/Def2TZVPP vibrational frequencies. Finally, geometry optimizations at the CCD/Def2TZVPP (chosen because of the availability of analytic gradients) and CCSD(T) levels are performed on the ground states of AgS^+ and $AgCS^+$ to examine the dependence of the structures on the level of theory. Because the results presented below generally involve only the Def2TZVPP basis set, they will usually be distinguished only by the level of theory used.

The thermodynamic accuracy of the results can be assessed by comparing them to several well known quantities. At the CCSD(T) (B3LYP) levels of theory, C—S and S—CS bond energies are calculated to be 7.05 (7.14) and 4.35 (4.70) eV, respectively. These compare reasonably well with the experimental bond energies of 7.37 ± 0.04 and 4.50 ± 0.04 eV, respectively.[62] Likewise, the average excitation energies of different spin states of Ag^+ are reproduced reasonably well. Experiment finds a $^1S(4d^{10})$ ground state for Ag^+, with a $^3D(5s^14d^9)$ state at 5.035 eV (average over all spin-orbit levels).[63] The two levels of theory find a ^1S ground state and yield values of 4.923 (4.672) eV for the ^3D state excitation energy, in good agreement with experiment. For the sulfur atom, the ^1D excited state is known to lie 1.145 eV above the ^3P ground state,[64] whereas theory provides excitation energies of 1.346 (1.668) eV.

III. THEORETICAL RESULTS

An understanding of the experimental results is facilitated by knowing the nature of the electronic states of the product AgS^+ and $AgCS^+$ species, along with the potential energy surfaces for reaction. The following section contains the theoretical results as obtained using the computational procedures described above.

A. AgS^+

At the B3LYP/Def2TZVPP level of theory, calculations predict a $^3\Sigma^-$ ground state for AgS^+. The ground state valence electron configuration is $(1\sigma)^2(2\sigma)^2(1\pi)^4(1\delta)^4(3\sigma)^2 \times (2\pi)^2$ where the 1σ orbital is largely S(3s), the 2σ and 1π orbitals are the metal-sulfur bonding orbitals, the 1δ are Ag(4d), the 3σ is largely Ag(5s), and 2π and 4σ are antibonding orbitals. Molecular parameters calculated at the CCD and CCSD(T) levels are similar to those given by B3LYP, Table I. CCSD(T)/B3LYP (B3LYP) calculations find $^3\Pi$ and $^1\Sigma^+$ excited states at 0.94 (0.98) and 1.46 (1.56) eV, respectively, above the ground state, Table I. These states have configurations of $(1\sigma)^2(2\sigma)^2(1\pi)^4(1\delta)^4(3\sigma)^1(2\pi)^3$ and $(1\sigma)^2(2\sigma)^2(1\pi)^4(1\delta)^4(3\sigma)^0(2\pi)^4$, respectively, with the relative energies reflecting the increased population of the antibonding 2π orbitals. Somewhat counterintuitively, the triplet states have longer bond lengths than the higher energy singlet state, with vibrational frequencies that follow this trend as well. These trends can be attributed to the antibonding character of the 3σ orbital, which lies along the bonding axis. These states can be thought of as interaction of a doubly ($^3\Sigma^-$) or singly ($^3\Pi$) occupied or empty ($^1\Sigma^+$) p orbital on S with the empty 5s orbital on Ag. Therefore, the two triplet states adiabatically dissociate to the ground state $Ag^+(^1S) + S(^3P)$ separated atoms, whereas the singlet state must correlate with the $Ag^+(^1S) + S(^1D)$ separated atoms, 1.145 eV higher in energy.

B. $AgCS^+$

The ground state of the silver thiocarbonyl cation is calculated to be a $^1\Sigma^+$ state corresponding to binding of $CS(^1\Sigma^+)$ to the ^1S ground state of Ag^+. As shown in Table II, the CS bond length in $AgCS^+$ ($^1\Sigma^+$) is slightly shorter than in free CS, by about 0.034 Å. Consistent with this finding, the vibrational frequency of the CS bond stretch increases by about 12%. Molecular parameters at the B3LYP, CCD, and CCSD(T) levels of theory are similar, Table II. The $AgCS^+$ molecule has a valence electron configuration of

TABLE II. Bond lengths, geometries, and state splittings for CS and $AgCS^+$ (geometry optimizations and frequency calculations performed at the B3LYP/Def2TZVPP, CCD/Def2TZVPP (bold), and CCSD(T)/Def2TZVPP (italics) levels of theory).

Species	State	r(Ag—C), (Å)	r(C—S) (Å)	∠AgCS (deg)	ν (cm^{-1})	E_{rel} (eV)[a] B3LYP	E_{rel} (eV)[a] CCSD(T)
CS	$^1\Sigma^+$		1.532, **1.527,** *1.544*		1311, **1362**	0.000	0.000
$AgCS^+$	$^1\Sigma^+$	2.084	1.498	180.0	205 (2), 251, 1467	0.000	0.000
		2.131	**1.495**	**180.0**	**204 (2), 239, 1514**		
		2.100	*1.510*	*180.0*			
	$^3A'$	2.072	1.585	125.7	130, 390, 918	3.537	3.951

[a]Relative single point energies calculated at the indicated level of theory using Def2TZVPP basis sets and B3LYP/Def2TZVPP geometries and corrected for zero point energies.

$(1\sigma)^2(2\sigma)^2(1\pi)^4(3\sigma)^2(2\pi)^4(1\delta)^4(4\sigma)^2$, where the 1σ, 2σ, and 1π orbitals are the carbon-sulfur bonding orbitals, the 3σ is a metal-carbon bond formed by donation of the HOMO of CS into a 5s-4d hybrid on Ag, the 2π are the backbonding interactions between the metal and the antibonding π orbitals on CS, the 1δ are Ag(4d), the 4σ is the other Ag(5s-4d) hybrid, and 3π and 5σ are Ag—C antibonding orbitals.

The ^3D excited state of Ag^+ interacts with CS to form a $^3A'$ excited state, Table II, with an excitation energy of 3.95 (3.54) eV, well below the atomic excitation energy of 4.92 (4.67) eV. In contrast with the linear geometry of the singlet ground state, the $^3A'$ state has a bent geometry with a slightly shorter Ag—C bond length and a longer CS bond with a commensurately lower CS bond stretch frequency. Using linear symmetry designations, the $^3A'$ state has a $(1\sigma)^2(2\sigma)^2(1\pi)^4(3\sigma)^2(2\pi)^4(1\delta)^4(4\sigma)^1(3\pi)^1$ configuration in which one of the antibonding 3π orbitals is singly occupied, which explains why the molecule is bent and why the CS molecule is altered so much.

C. Singlet potential energy surface

The reaction coordinate diagram for reaction of CS_2 with Ag^+ in the singlet (blue) and triplet (red) spin states is shown in Fig. 1. The energies used in the diagram are calculated at the CCSD(T)//B3LYP level of theory and will be used throughout the following discussion. Geometries of intermediates and products of reactions (1) and (2) are shown in Fig. 2 in the same order as one moves across Fig. 1 with relative energies and structural parameters provided in Table III. All of the species are planar.

Along the singlet surface, the initial interaction of $Ag^+(^1S)$ with $CS_2(^1\Sigma_g^+)$ leads to the $Ag^+(SCS)$ ($^1A'$) complex bound by 1.16 eV with respect to the reactants. This species can be thought of as the donation of the nonbonding in-plane π orbital of CS_2 into the empty 5s orbital on Ag^+

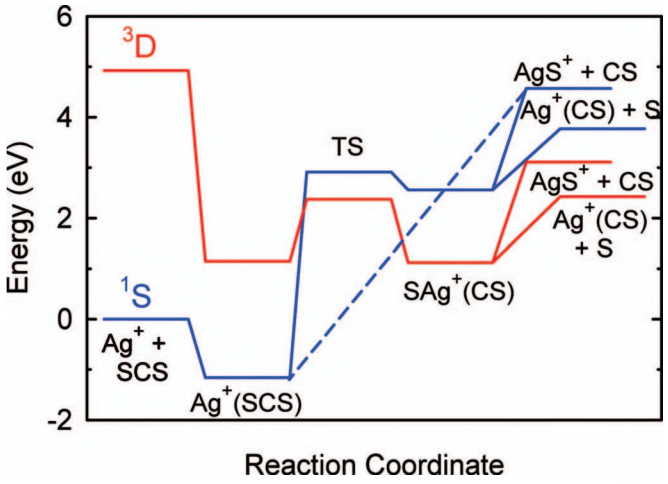

FIG. 1. Reaction coordinate diagram for reaction of Ag^+ in singlet (blue line) and triplet (red line) states with CS_2. The dashed line shows the direct dissociation of $Ag^+(SCS)$ to AgS^++CS. All energies are calculated at the CCSD(T)//B3LYP level including zero point energies.

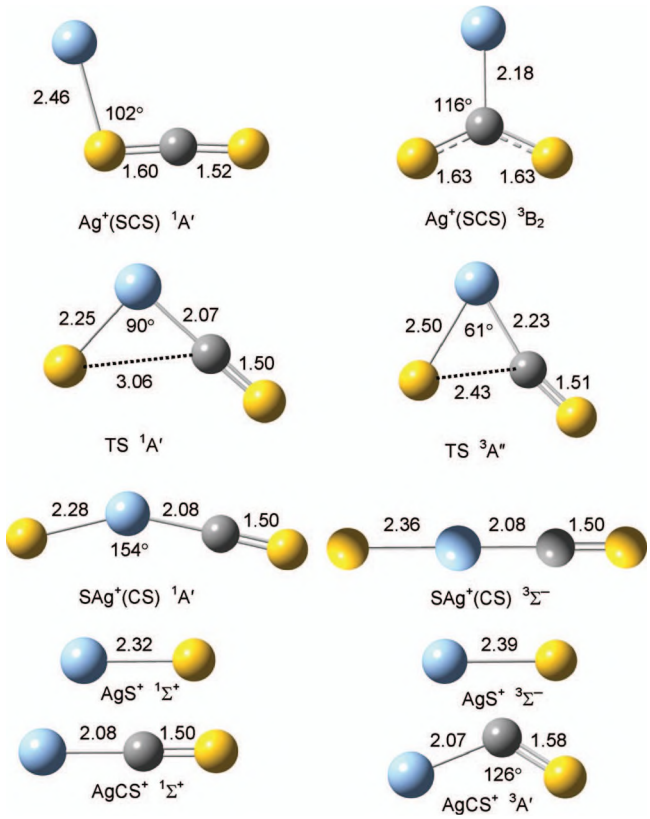

FIG. 2. Singlet and triplet spin intermediates, TSs, and products calculated at the B3LYP/Def2TZVPP level of theory. Species match the order in the reaction coordinate diagram of Fig. 1. Bond lengths are shown in angstrom. All species are planar. Atoms are color coded as blue for silver, gray for carbon, and yellow for sulfur.

TABLE III. Geometric parameters, vibrational frequencies, and relative energies for reactants, products, intermediates, and transitions states for reaction of Ag^+ with CS_2. (All geometric parameters are calculated at the B3LYP/Def2TZVPP level of theory.)

Species	State	r(AgS) (Å)	r(AgC) (Å)	r(CS) (Å)	∠AgSC, ∠SAgC (deg)	∠SCS, ∠AgCS (deg)	ν (cm^{-1})	E_{rel} [a] (eV)
$Ag^+ + CS_2$	$^1\Sigma^+_g$			1.553 (2)		180.0[b]	408 (2), 678, 1561	0.000(0.000)
$Ag^+(SCS)$	$^1A'$	2.462		1.597,1.523	102.2[b]	175.1[b]	66, 215, 301, 425, 655, 1540	−1.157(−1.298)
	$^1\Sigma^+$	2.499		1.571,1.527	180.0[b]	180.0[b]	−144 (2), 129, 318 (2), 689, 1585	−0.541(−0.580)
	$^3B_2$		2.182	1.630 (2)		128.8,[b]115.6(2)[c]	106, 157, 286, 356, 797, 1035	1.147(0.876)
	$^1A''$	2.456		1.636,1.616	103.7[b]	138.4[b]	82, 134, 166, 300, 640, 999	1.934(1.529)
CP1	$^3A''$	2.495	2.222	1.518,2.349	54.5,[b]59.4[c]	130.5,[b]163.4[c]	−391, 130, 197, 258, 290, 1318	2.349(2.316)
CP2	$^1A'$	2.353		1.500,2.575	96.9[b]	173.1[b]	−233, 53, 219, 234, 315, 1392	2.509(2.426)
CP1	$^1A'$	2.212	2.044	1.502,2.600	49.5,[b]75.2[c]	149.7,[b]155.0[c]	−293, 129, 225, 320, 379, 1414	2.727(2.735)
$SAgCS^+$ (TS)	$^3A''$	2.505	2.234	1.514,2.431	53.8,[b]61.4[c]	129.8,[b]165.4[c]	−205, 120, 130, 190, 219, 1341	2.372(2.312)
	$^1A'$	2.251	2.072	1.496,3.055	42.7,[b]89.8[c]	133.9,[b]178.6[c]	−181, 108, 188, 245, 327, 1467	2.912(2.985)
$SAgCS^+$	$^3\Sigma^-$	2.360	2.085	1.500	180.0[c]	180.0[c]	42 (2), 228 (2), 236, 275, 1461	1.120(1.171)
	$^3\Pi$	2.374	2.114	1.498	180.0[c]	180.0[c]	39, 46, 211, 227, 239, 261, 1466	2.081(2.107)
	$^1A'$	2.278	2.081	1.499	154.1[c]	178.9[c]	47, 214, 232, 251, 324, 1462	2.557(2.636)
	$^1\Sigma^+$	2.288	2.100	1.499	180.0[c]	180.0[c]	−68, 57, 181, 242, 251, 313, 1460	2.527(2.670)
$AgS^+ + CS$	$^3\Sigma^- + {}^1\Sigma^+$	2.392		1.532			237, 1311	3.110(3.182)
$AgCS^+ + S$	$^1\Sigma^+ + {}^3P$		2.084	1.498		180.0[c]	205 (2), 251, 1467	2.423(2.613)

[a]Relative energies calculated at CCSD(T)/Def2TZVPP//B3LYP/Def2TZVPP (B3LYP/Def2TZVPP) levels of theory, corrected for zero point energies. Absolute calculated energies for the ground state reactants are 979.981 320 (981.296 821) E_h, including zero point energies.
[b]∠AgSC and ∠SCS.
[c]∠SAgC and ∠AgCS.

(where the latter undergoes s-d hybridization to minimize the repulsion). Therefore, the structure has a bent geometry. In this complex, the CS_2 ligand is distorted by stretching the CS bond closer to the metal ion (and shortening the other CS bond) and bending the ligand to 175° from linear. A linear variant of this species is located 0.62 eV higher in energy but has a degenerate imaginary frequency (144 cm^{-1}) associated with AgSC bending motions that allow it to rearrange to the lower energy bent isomer. A $^1A''$ state is also located lying 3.09 eV above the $^1A'$ ground state. Here, the CS_2 ligand is much more highly distorted, with long CS bond lengths and an ∠SCS bond angle of 138°. This is because there is a singly occupied π-like orbital that lies out of the plane of the molecule.

From the encounter complex, reaction can take place by oxidative addition of a CS bond to the silver center, leading to TS($^1A'$). Because of the closed shell character of both reagents, this step requires considerable energy, 4.07 eV above the Ag^+(SCS) intermediate. The imaginary frequency of 181 cm^{-1} corresponds to elongation of the CS bond. This TS has slightly shorter AgS and AgC bond lengths and a smaller ∠SAgC bond angle compared to the SAg^+(CS) ($^1A'$) intermediate that is then formed. The SAg^+(CS) intermediate is only 0.36 eV below the TS, and has a large ∠SAgC bond angle of 154°, Fig. 2. Relaxed potential energy scans, in which the likely reaction coordinate is systematically varied while all other coordinates are allowed to optimize, verify that the TS connects the two adjacent intermediates. The SAg^+(CS) intermediate has a slightly shorter AgS bond compared to the $^1\Sigma^+$ state of the AgS^+ product and a similar geometry compared to the $^1\Sigma^+$ state of the Ag^+(CS) product, Fig. 2. This intermediate can be viewed as donation of the σ(CS) lone pair of electrons (the HOMO) into the 3σ s-d hybrid orbital of AgS^+ ($^1\Sigma^+$). The bent geometry occurs because one of the pπ orbitals on the sulfur ligand is empty, permitting distortion in that plane. A linear version of the SAg^+(CS) intermediate (a $^1\Sigma^+$ state) is calculated to be essentially isoenergetic (within 0.03 eV after zero point energy corrections) but has an imaginary frequency of 68 cm^{-1} corresponding to the bend that takes it to the $^1A'$ state, Table III.

From the SAg^+(CS) ($^1A'$) intermediate, cleavage of the metal ligand bonds leads to both $AgS^+ + CS$ and Ag^+(CS) + S product channels. If spin is conserved, the accessible product channel for reaction (1) is $AgS^+(^1\Sigma^+) + CS(^1\Sigma^+)$ and for reaction (2) is $Ag^+(CS)(^1\Sigma^+) + S(^1D)$, both excited state asymptotes, Fig. 1. It is also possible to form $AgS^+(^1\Sigma^+) + CS(^1\Sigma^+)$ directly from the initially formed Ag^+(SCS) ($^1A'$) intermediate. Calculations of AgS^+—CS bond cleavage from this species verify that dissociation occurs without any barriers in excess of the product asymptote.

D. Triplet potential energy surface

Reaction along the triplet surface starts much higher in energy as the ^3D state of Ag^+ is calculated to lie 4.92 eV (5.03 eV experimental) above the ground state. The lowest energy Ag^+(SCS) complex having triplet spin has C_{2v} symmetry ($^3B_2$ state) with the metal ion bound to the carbon, Fig. 2. The CS_2 ligand is considerably distorted, with CS bond lengths increasing from 1.553 to 1.630 Å and the SCS bond angle changing from linear to 129°. This intermediate is bound by 3.77 eV relative to the triplet state reactant asymptote.

Oxidative addition of a CS bond to the silver center leads to TS($^3A''$), Fig. 2. The imaginary frequency of 205 cm^{-1} corresponds to the expected CS stretching motion. This TS lies 1.22 eV above the Ag^+(SCS) ($^3B_2$) intermediate and 1.25 eV above the SAg^+(CS) ($^3\Sigma^-$) intermediate then

formed. Relaxed potential energy scans verify that the $^3A''$ TS connects the two adjacent intermediates. Notably, the triplet TS and $SAg^+(CS)$ intermediate lie *below* the corresponding singlet species, by 0.54 and 1.44 eV, respectively. The linear $^3\Sigma^-$ intermediate has a slightly shorter AgS bond compared to the $^3\Sigma^-$ state of the AgS^+ product, and a comparable AgC bond length compared to the $^3A'$ state of the $Ag^+(CS)$ product, Fig. 2. The $SAg^+(CS)$ intermediate can be viewed as donation of the σ(CS) lone pair of electrons into the 3σ s-d hybrid orbital of AgS^+ ($^3\Sigma^-$). Unlike the singlet state, distortion from a linear geometry increases the energy because both $p\pi$ orbitals on the S ligand are singly occupied. In addition, a $^3\Pi$ state of the $SAg^+(CS)$ intermediate was found to lie 0.96 eV above the $^3\Sigma^-$ state, matching the excitation energy for the AgS^+ ($^3\Pi$) product of 0.94 eV, Table I.

From the $SAg^+(CS)$ ($^3\Sigma^-$) intermediate, spin-conserving cleavage of the metal-ligand bonds can lead to $AgS^+(^3\Sigma^-)+CS(^1\Sigma^+)$ as well as $Ag^+(CS)$ ($^1\Sigma^+$)+S(^{3}P). These are the ground states for both product channels. From the initially formed $Ag^+(SCS)$ ($^3B_2$) intermediate, cleavage of the C—S bond leads to bond insertion forming the $SAg^+(CS)$ intermediate along the path already discussed. This occurs because of the proximity of the silver cation to the elongating CS bond. Furthermore, it is found that if $Ag^+(^3D)$ approaches the SCS end on, the interaction is repulsive. Thus, there is no low-energy pathway for formation of $AgS^+(^3\Sigma^-)+CS(^1\Sigma^+)$ directly from the $Ag^+(SCS)$ encounter complex along the triplet surface.

E. Singlet/triplet surface crossing

As noted above, formation of the ground state products of reactions (1) and (2) from ground state reactants requires changing spin from singlet to triplet. The efficiency of this spin change will be influenced by the extent of spin-orbit coupling (enhanced by the presence of both the heavy metal and sulfur) as well as the character of the seam over which the two spin surfaces interact. To approximate the character of the crossing seam, a relaxed potential energy surface scan along a likely region of coordinate space for each spin state is conducted and then the energies of the other spin state at the same geometries are also calculated, as per the approach of Yoshizawa *et al.*[65] From Fig. 1, it seems likely that the crossing region lies between the $Ag^+(SCS)$ intermediate and the TS for CS bond insertion. Therefore, we examined the coordinate associated with bending the SAgC bond angle.

Results of these calculations are shown in Fig. 3, with geometries of the approximate crossing points (CPs) shown alongside. Energies and approximate geometries for the CPs are listed in Table III. Along the optimized singlet surface for bending, CP1($^1A'/^3A''$) occurs just before TS($^1A'$) at an energy of 2.73 eV. Along the optimized triplet surface, CP1($^3A''/^1A'$) lies very close to TS($^3A''$) at an energy of 2.35 eV. A key observation is that the crossing seam lies in a region near the TSs for bond insertion, and hence a region of the potential energy surface where the atoms are unlikely to spend much time. Note also that these energies are close to

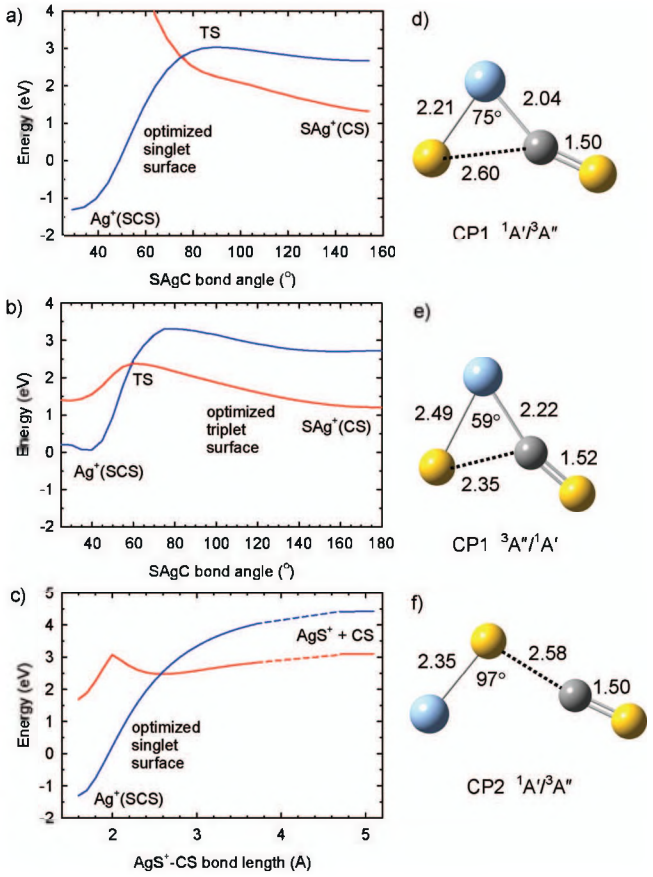

FIG. 3. Relaxed potential energy surface scans at the B3LYP/Def2TZVPP level of theory for conversion from $Ag^+(SCS)$ to $SAg^+(CS)$ intermediates (parts a and b) and for dissociation of $Ag^+(SCS)$ to AgS^++CS (part c). Results are shown for optimization along the singlet (parts a and c) and triplet (part b) surfaces with single point energies at the same geometries for the other spin state. Geometries of the approximate crossing points (CP) between the surfaces are shown in parts d–f. Bond lengths are shown in angstrom.

the energy of the $Ag^+(CS)(^1\Sigma^+)$+S(^{3}P) product asymptote, 2.42 eV, and not far below that for $AgS^+(^3\Sigma^-)+CS(^1\Sigma^+)$, 3.11 eV, Table III.

We also examine the pathway for forming AgS^++CS directly from the initially formed $Ag^+(SCS)(^1A')$ intermediate. Here energies for the triplet surface at the optimized geometries for AgS^+—CS dissociation along the singlet surface are calculated, Fig. 3(c). We find that the crossing point CP2($^1A'/^3A''$) occurs when the AgS^+—CS bond has lengthened to about 2.58 Å, at an energy of 2.51 eV. This energy is well above the ground state $Ag^+(SCS)(^1A')$ intermediate and similar to the energies of the CP1 crossing points.

IV. EXPERIMENTAL RESULTS

Reaction of Ag^+ with CS_2 yields two major products, AgS^+ and $AgCS^+$, formed in reactions (1) and (2), along with the charge transfer product ion, CS_2^+. Unlike the flow tube studies of Bohme and co-workers,[27] no $Ag^+(CS_2)$ adducts are observed because the single collision conditions used here do not allow the collisional relaxation necessary to form such adducts. Figure 4 shows results obtained for Ag^+ ions produced using the flow tube discharge source with no quenching gas added to the flow tube (open symbols). Under these

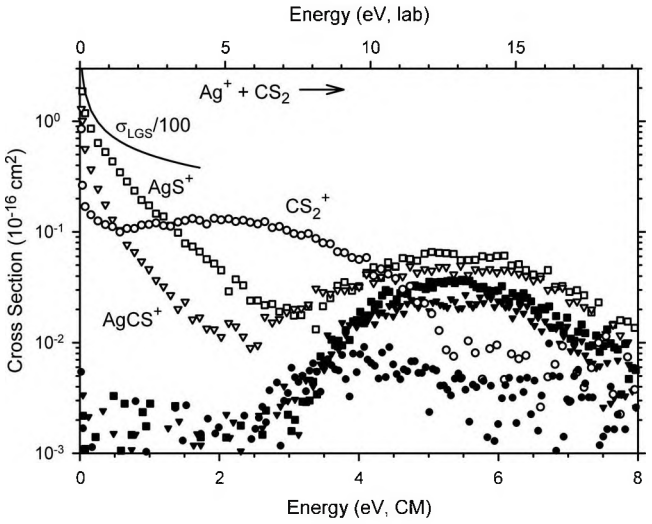

FIG. 4. Product cross sections for the reaction of CS_2 with Ag^+ formed without cooling (open symbols) or cooled by reaction with O_2 (closed symbols) as a function of CM energy (lower axis) and laboratory energy (upper axis). Cross sections for formation of AgS^+ (squares), $AgCS^+$ (inverted triangles), and CS_2^+ (circles) are shown.

conditions, all three product cross sections have large magnitudes at low energy, decline with increasing energy before rising again at higher collision energies. Thus all three reactions appear to take place via barrierless, exothermic pathways, as well as endothermic pathways. The energy dependence of the low energy feature below about 0.4 eV is consistent with the Langevin–Gioumousis–Stevenson collision cross section for ion-molecule reactions,[66] $\sigma_{LGS}(E) = (\pi q/4\pi\varepsilon_0)(2\alpha/E)^{1/2}$, where q is the charge on the ion, ε_0 is the permittivity of vacuum, E is the collision energy, and α is the polarizability volume of CS_2, 8.74 Å^3.[67]

The low energy features in these cross sections are likely to be associated with electronically excited states of Ag^+. The presence of excited states is confirmed by examining the charge transfer reaction, which has a finite cross section at low energies and then rises slowly with increasing energy before reaching a maximum near 2 eV. The ionization energies of CS_2 and Ag are 10.073 ± 0.005 (Ref. 68) and 7.576 23 eV,[69] respectively, such that the charge transfer reaction involving ground states species is endothermic by 2.497 ± 0.005 eV. The lowest energy excited state is the $^3D_3$ spin-orbit level, which lies 4.856 eV above the ^1S ground state, such that all excited states of Ag^+ have sufficient energy to react exothermically by charge transfer with CS_2. It seems likely that the dominant excited state present is the ^3D state, which is both spin and parity forbidden to radiate to the ground state. Note that the experimental cross section magnitudes are only about 1% of the σ_{LGS} prediction, Fig. 4, suggesting that the population of the excited states could be as little as 1% of the reactant ion beam (which assumes that they react with 100% efficiency).

The presence of excited states is further confirmed by admitting small amounts of O_2 into the flow tube to quench the excited states. As demonstrated previously,[38] oxygen reacts efficiently with the excited states of Ag^+ in an exothermic process. Under source conditions that include the O_2 quenching gas, the exothermic features in the AgS^+, $AgCS^+$, and CS_2^+ cross sections all decrease by two to three orders of magnitude, whereas the endothermic features in the AgS^+ and $AgCS^+$ cross sections remain and only a small cross section for CS_2^+ is observed, Fig. 4 (closed symbols). These cross sections correspond to reaction of pure $Ag^+(^1S)$.

TABLE IV. Summary of parameters in Eqs. (3) and (4) used to analyze the cross sections for reactions (1) and (2) (uncertainties in parentheses, where values for E_0 are two standard deviations).

Reaction	σ_0	n	E_0 (eV)	$D_0(Ag^+\text{-X})$ (eV)
$Ag^+ + CS_2 \rightarrow AgS^+ + CS$	0.09(0.02)	1.3(0.2)	3.23(0.12)[a]	1.27(0.13)
	0.29(0.30)	0.8(0.4)	3.10(0.09)[b]	1.40(0.12)
$\rightarrow AgCS^+ + S$	0.05(0.01)	1.3(0.3)	2.92(0.16)[a]	1.58(0.21)
	0.50(0.49)	0.8(0.4)	2.52(0.11)[b]	1.98(0.14)

[a]Single channel fit using Eq. (3).
[b]Competitive fit using Eq. (4) with a loose (PSL) TS for reaction (2). Values for $m = 1.0$ and 1.5 are equivalent except $n = 1.3 \pm 0.3$ when $m = 1.5$.

For reaction of ground state $Ag^+(^1S)$, the AgS^+ and $AgCS^+$ product cross sections rise from apparent thresholds near 3 eV. The apparent threshold for formation of CS_2^+ is slightly lower (Fig. 4, closed circles) and consistent with the expected endothermicity for charge transfer of 2.497 ± 0.005 eV. Above about 5 eV, the AgS^+ and $AgCS^+$ cross sections begin to decline. This behavior can be attributed to dissociation of the products, the overall process (6), which can start at $D_0(SC\text{—}S) = 4.50 \pm 0.04$ eV.[62]

$$Ag^+ + CS_2 \rightarrow Ag^+ + CS + S. \quad (6)$$

The onset for this dissociation appears to be delayed somewhat from the thermodynamic value of 4.5 eV, which indicates that the reactions take place by a pathway that deposits excess energy in translation rather than internal degrees of freedom of the ionic products.

Careful analysis of the threshold regions for the cross sections of reactions (1) and (2) yields the E_0, σ_0, and n values summarized in Table IV. The reaction channels are analyzed independently when using Eq. (3). These results indicate that the threshold energy for reaction (2) is about 0.3 eV smaller than that for reaction (1) even though the latter has a larger cross section. When these channels are analyzed as competitive reactions using the $SAg^+(CS)$ ($^3\Sigma^-$) intermediate as the EM, Eq. (4) is able to reproduce the data nicely throughout the threshold region, up to 5 eV, slightly beyond where reaction (6) can begin, as shown in Fig. 5. The model reproduces the shapes of both the AgS^+ and $AgCS^+$ cross sections well, even though the energy dependences are clearly distinct and despite the fact that the value of n used is the same for both channels in the competitive analysis. Conventionally, the value of the parameter m in Eq. (4) is held to unity, however, here values of $m = 1.0$ and 1.5 were both tried and yielded very similar fits (the value of n increases from 0.8 to 1.3), with essentially identical threshold energies. As discussed previously for the reaction of V^+ with CS_2,[14] spin inversion can change the cross-section shape. Because more energetic reactants pass through the surface crossing region more rapidly, the ability of the electrons to adjust to different configurations along the reaction coordinate is reduced.

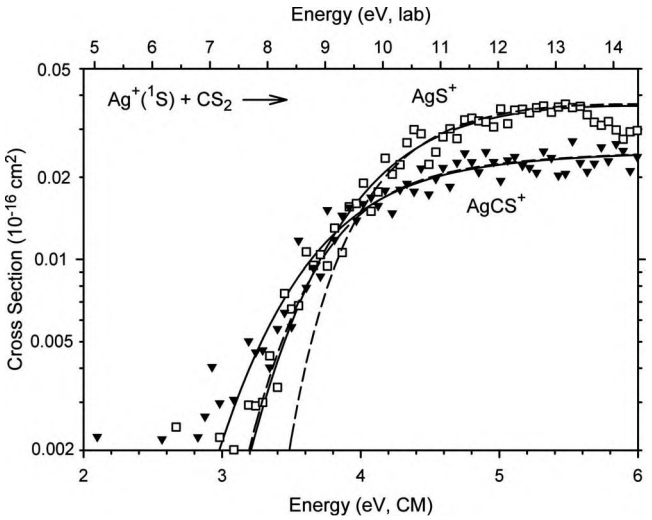

FIG. 5. Cross sections for the reaction of $Ag^+(^1S)$ with CS_2 to form AgS^+ (open squares) and $AgCS^+$ (closed inverted triangles) as a function of CM energy (lower axis) and laboratory energy (upper axis). Solid lines show the competitive model cross sections given by Eq. (4) and the parameters given in Table IV ($m=1.0$). Dashed lines show these models in the absence of experimental kinetic energy distributions for reactants at 0 K.

Thus, a spin-forbidden path can exhibit a reaction efficiency that varies approximately as $E^{-1/2}$, which can be included in the data analysis by using a value of 1.5 for the parameter m. Because reactions (1) and (2) are spin forbidden, this alternate value of m is included in the present data analysis.

As for the independent channel analysis, the competitive analysis yields thresholds for the two reactions that differ appreciably, Table IV, with that for $AgCS^+$ being lower by 0.58 ± 0.01 eV. Even though the $AgCS^+$ cross section has a lower threshold, its magnitude remains the same or slightly smaller than the AgS^+ cross section except at the lowest energies, Fig. 5. Furthermore, the model shown requires that this channel be scaled up by a factor of 1.8 ± 0.1 (as reflected by the different σ_0 values in Table IV). The $AgS^+ + CS$ channel is statistically favored because it has four rotational and two vibrational degrees of freedom whereas the $AgCS^+ + S$ channel has only two rotations and four vibrations. The 1.8 scaling factor used can be rationalized by the differences in the electronic degeneracies of the two channels: three for the $AgS^+(^3\Sigma^-) + CS(^1\Sigma^+)$ channel versus nine for the $Ag^+(CS)(^1\Sigma^+) + S(^3P)$ channel, which introduces a scaling factor of 3.

Finally, it is also possible that the $AgS^+ + CS$ channel is favored compared to $Ag^+(CS) + S$ formation because the former can be produced from the initially formed $Ag^+(SCS)$ intermediate by cleaving the AgS^+—CS bond, without the need for bond insertion. Such an alternate pathway could increase the probability of reaction (1) relative to reaction (2), which could also contribute to the scaling factor found empirically. Analysis of the data explicitly including such a possibility is beyond the capability of the analysis software, however, the presence of this alternative pathway does not change the fact that the two channels are still coupled. Because the rates of reaction are most sensitive to the number of states at the TS and relatively insensitive to the density of states of the EM, Eq. (5), the competition between reactions (1) and (2) relies primarily on the properties of the products. As these properties are explicitly accounted for in the competitive analysis above, the presence of the additional pathway for AgS^+ formation is unlikely to change the thermodynamics obtained.

The E_0 values can be converted to the Ag^+—S and Ag^+—CS bond strengths at 0 K using Eq. (7), where X can represent either S or CS. These values are also provided in Table IV.

$$D_0(Ag^+ — X) = D_0(SC — S) - E_0. \quad (7)$$

The values obtained from the competitive modeling differ only somewhat from those obtained from the independent analyses, where the latter have been reported previously.[23] We believe that the more sophisticated competitive modeling, which reproduces both cross sections simultaneously, provides the most accurate threshold values in addition to being more precise. Our best values are taken as the average of the competitive fits using $m=1.0$ and 1.5: $D_0(Ag^+—S) = 1.40 \pm 0.12$ eV and $D_0(Ag^+—CS) = 1.98 \pm 0.14$ eV, where the uncertainties are two standard deviations. Uncertainties include variations associated with multiple data sets, values of m, frequencies of reactants and products ($\pm 10\%$), time available for reaction (factor of 2), absolute energy of the EM (± 0.3 eV), and the uncertainty in the absolute zero of energy (± 0.02 eV).

V. DISCUSSION

A. Thermochemistry

After correcting for basis set superposition errors at the full counterpoise limit,[70,71] the calculated bond energy of the AgS^+ ($^3\Sigma^-$) ground state is 1.50 eV at the B3LYP level of theory, considerably higher than the 1.17, 1.18, and 1.19 eV values calculated at the CCSD(T)//B3LYP, CCSD(T)//CCD, and CCSD(T) levels of theory, respectively, Table V. All values are in reasonable agreement with the experimental

TABLE V. Experimental and theoretical bond energies (eV).

Bond	Exp.	B3LYP[a]	CCSD(T)//B3LYP[a]	CCSD(T)//CCD[a]	CCSD(T)[a]
Ag^+—S	1.40 ± 0.12	1.505 (1.518)	1.171 (1.245)	1.180 (1.245)	1.194 (1.264)
Ag^+—CS	1.98 ± 0.14	2.078 (2.087)	1.834 (1.932)	1.835 (1.925)	1.889 (1.984)
MAD[b]		0.10 ± 0.01	0.19 ± 0.06	0.18 ± 0.05	0.15 ± 0.08

[a]In all cases, theoretical values are obtained at the level shown using the Def2TZVPP basis sets. Values are corrected for zero point energies and for basis set superposition errors in the full counterpoise limit. Values without counterpoise corrections are in parentheses.
[b]Mean absolute deviation from experimental values.

bond energy of 1.40 ± 0.12 eV. Similar discrepancies (0.2–0.3 eV) are found in the cases of RhS^+ and PdS^+ compared to the CCSD(T) bond energies.[25,26] If it is assumed that the product formed is the AgS^+ ($^1\Sigma^+$) excited state, corresponding to spin conservation in the exit channel, the agreement with theory is unacceptable. This species has calculated bond energies of 0.53 eV (B3LYP), 0.23 eV (CCSD(T)//B3LYP), and 0.24 eV (CCSD(T)//CCD), well below the experimental value. Thus, formation of the AgS^+ product must occur by crossing from the singlet spin of the reactants to the triplet spin of the products in reaction (1).

For the silver thiocarbonyl cation, the $^1\Sigma^+$ ground state is bound by 2.08, 1.83, 1.84, and 1.89 eV at the B3LYP, CCSD(T)/B3LYP, CCSD(T)/CCD, and CCSD(T) levels of theory, respectively, with counterpoise corrections. These values are in reasonable agreement with the experimental value of 1.98 ± 0.14 eV, if this is assumed to form ground state $Ag^+(CS)$ ($^1\Sigma^+$)+S(^{3}P) products, a spin-forbidden process. If the measured threshold is assumed to correspond to the lowest energy spin-allowed process, formation of $Ag^+(CS)$ ($^1\Sigma^+$)+S(^{1}D), then the bond energy derived would be 3.12 eV, much higher than the theoretical values. Thus, we conclude that reaction (2) must also occur via a spin-forbidden pathway forming ground state products.

Theory indicates that the Ag^+—CS bond is stronger than the Ag^+—S bond by 0.57–0.66 eV (Table V), in good agreement with experiment which finds a difference of 0.58 eV from the competitive analysis (0.31 eV from the independent channel analysis). This agreement is better than that obtained for the sulfide and thiocarbonyl cations of the other late second-row transition metals, Ru^+, Rh^+, and Pd^+.[24–26] Part of the reason for the better agreement is that the metal-ligand bonding in the MS^+ and $M^+(CS)$ molecules is distinct for M^+=Ru^+, Rh^+, and Pd^+, i.e., covalent for MS^+ and dative for $M^+(CS)$, whereas for AgS^+ and $Ag^+(CS)$, the ground states are both formed by donation of a lone pair of electrons on the ligand into the empty 5s orbital of Ag^+(^{1}S).

B. Reaction mechanism

The reaction coordinate diagram of Fig. 1 shows clearly that reactions (1) and (2) can occur by insertion of the silver cation into a CS bond of CS_2 followed by simple cleavage of one of the metal ligand bonds. Alternatively, the initially formed $Ag^+(SCS)$ ($^1A'$) intermediate can also form the AgS^++CS products by cleavage of the AgS^+—CS bond. The experimental results analyzed correspond to reaction of ground state Ag^+(^{1}S), and comparison of experimental and theoretical thermochemistry indicates that the ground state AgS^+($^3\Sigma^-$)+CS($^1\Sigma^+$) and $Ag^+(CS)$ ($^1\Sigma^+$)+S(^{3}P) products are formed. Thus, the observed reactivity is spin forbidden for both channels and involves transfer from the singlet surface evolving from ground state reactants to the triplet surface leading to ground state products.

Comparison of the results to those for other late second-row transition metal cations is illuminating. We find that the maximum cross sections for both products observed here are about 30 times smaller than those observed for reaction of Ru^+, Rh^+, and Pd^+ with CS_2.[24–26] In all four systems, spin changes are required to form ground state MS^+ products from the ground state reactants, therefore spin conservation alone cannot explain this variation in reaction efficiency. However, the location of the crossing points between the spin states is distinct in the silver system compared to M^+=Ru^+, Rh^+, and Pd^+. As discussed above for M^+=Ag^+, these crossings occur in the vicinity of the TS for CS bond insertion or as the AgS^+—CS bond is broken. Therefore, it seems likely that the system spends relatively little time where the spin-orbit coupling between the singlet and triplet surfaces can occur. In contrast with the Ag^+ system, the CPs for the other three metal cations occur primarily in the vicinity of the $SM^+(CS)$ intermediates as well as along the pathway for dissociation to MS^++CS.[24–26] Thus, these systems can spend relatively more time exploring the potential energy surface near the crossing points, compared to the silver system. These comparisons illustrate that the heavy metal-sulfur systems can react via spin-forbidden processes, but the efficiency of such reactions is greatly influenced by the details of the crossing seam between the surfaces of different spin.

ACKNOWLEDGMENTS

Professor D. Schröder and Professor H. Schwarz are thanked for their support and guidance when these data were taken. This work was supported by the Fonds der Chemischen Industrie and the National Science Foundation (PBA, Grant No. CHE-0748790). In addition, we thank the Center for High Performance Computing at the University of Utah for the generous allocation of computer time.

[1] D. Fărcaşiu, A. Ghenciu, and J. Q. Li, J. Catal. **158**, 116 (1996); A. P. Raje, S.-J. Liaw, R. Srinivasan, and B. H. Davis, Appl. Catal., A **150**, 297 (1997); N. Allali, E. Prouzet, A. Michalowicz, V. Gaborit, A. Nadiri, and M. Danot, *ibid.* **159**, 333 (1997); M. M. Mdleleni, T. Hyeon, and K. S. Suslick, J. Am. Chem. Soc. **120**, 6189 (1998); A. C. B. dos Santos, P. Grange, and A. C. Faro, Jr., Appl. Catal., A **178**, 29 (1999); J.-P. Janssens, D. A. van Langeveld, and J. A. Moulijn, *ibid.* **179**, 229 (1999).
[2] For a comparison of hydrodechlorination and hydrodesulfurization selectivities and activities of MS M=V—Ni; Mo—Pd, W, Ir, Pt, see J. Frimmel and M. Zaradzil, J. Catal. **167**, 286 (1997).
[3] T. Tani, Imaging Sci. J. **55**, 65 (2007).
[4] Z. Wang, T. Kadohira, T. Tada, and S. Watanabe, Nano Lett. **7**, 2688 (2007).
[5] K. Terabe, T. Hasegawa, C. Liang, and M. Aono, Sci. Technol. Adv. Mater. **8**, 536 (2007).
[6] M. Morales-Masis, S. J. van der Molen, W. T. Fu, M. B. Hesselberth, and J. M. van Ruitenbeek, Nanotechnology **20**, 095710 (2009).
[7] L. Tymecki, E. Zwierkowska, S. Glab, and R. Knocki, Sens. Actuators B **482**, 488 (2003).
[8] S. Satokawa, Y. Kobayashi, and H. Fujiki, Appl. Catal., B **56**, 51 (2005).
[9] C. Leiggener, D. Bruhwiler, and G. Calzaferri, J. Mater. Chem. **13**, 1969 (2003).
[10] L. Jonas, C. Bloch, R. Zimmermann, V. Stadie, G. E. Gross, and S. G. Schad, Ultrastruct. Pathol. **31**, 379 (2007).
[11] A. A. Levchenko, C. K. Yee, A. N. Parikh, and A. Navrotsky, Chem. Mater. **17**, 5428 (2005).
[12] M. Arita, J. Phys. Chem. Solids **68**, 1730 (2007).
[13] I. Kretzschmar, D. Schröder, H. Schwarz, C. Rue, and P. B. Armentrout, J. Phys. Chem. A **102**, 10060 (1998).
[14] C. Rue, P. B. Armentrout, I. Kretzschmar, D. Schröder, J. N. Harvey, and H. Schwarz, J. Chem. Phys. **110**, 7858 (1999).
[15] D. Schröder, I. Kretzschmar, H. Schwarz, C. Rue, and P. B. Armentrout, Inorg. Chem. **38**, 3474 (1999).
[16] S. Bärsch, I. Kretzschmar, D. Schröder, H. Schwarz, and P. B. Armentrout, J. Phys. Chem. A **103**, 5925 (1999).

[17] I. Kretzschmar, D. Schröder, H. Schwarz, C. Rue, and P. B. Armentrout, J. Phys. Chem. A **104**, 5046 (2000).
[18] C. Rue, P. B. Armentrout, I. Kretzschmar, D. Schröder, and H. Schwarz, J. Phys. Chem. A **105**, 8456 (2001).
[19] C. Rue, P. B. Armentrout, I. Kretzschmar, D. Schröder, and H. Schwarz, Int. J. Mass Spectrom. **210–211**, 283 (2001).
[20] C. Rue, P. B. Armentrout, I. Kretzschmar, D. Schröder, and H. Schwarz, J. Phys. Chem. A **106**, 9788 (2002).
[21] I. Kretzschmar, D. Schröder, H. Schwarz, and P. B. Armentrout, Int. J. Mass Spectrom. **228**, 439 (2003).
[22] I. Kretzschmar, D. Schröder, H. Schwarz, and P. B. Armentrout, Int. J. Mass Spectrom. **249–250**, 263 (2006).
[23] I. Kretzschmar, D. Schröder, H. Schwarz, and P. B. Armentrout, Adv. Met. Semicond. Clusters **5**, 347 (2001).
[24] P. B. Armentrout and I. Kretzschmar, "Guided ion beam and theoretical studies of the reaction of Ru^+ with CS_2 in gas-phase: Thermochemistry of Ru^+C, Ru^+S, and Ru^+CS," PhysChemChemPhys (submitted).
[25] P. B. Armentrout and I. Kretzschmar, J. Phys. Chem. A **113**, 10955 (2009).
[26] P. B. Armentrout and I. Kretzschmar, Inorg. Chem. **48**, 10371 (2009).
[27] P. Cheng, G. K. Koyanagi, and D. K. Bohme, J. Phys. Chem. A **110**, 2718 (2006).
[28] P. B. Armentrout, Science **251**, 175 (1991).
[29] D. R. Yarkony, J. Phys. Chem. **100**, 18612 (1996).
[30] D. Schröder, H. Schwarz, and S. Shaik, in *Metal-Oxo and Metal-Peroxo Species in Catalytic Oxidations*, edited by B. Meunier (Springer, Berlin, 2000), pp. 91–123.
[31] R. Poli and J. N. Harvey, Chem. Soc. Rev. **32**, 1 (2003).
[32] K. M. Ervin and P. B. Armentrout, J. Chem. Phys. **83**, 166 (1985).
[33] R. H. Schultz and P. B. Armentrout, Int. J. Mass Spectrom. Ion Process. **107**, 29 (1991).
[34] F. Muntean and P. B. Armentrout, J. Chem. Phys. **115**, 1213 (2001).
[35] Y.-M. Chen, J. L. Elkind, and P. B. Armentrout, J. Phys. Chem. **99**, 10438 (1995).
[36] M. R. Sievers, Y.-M. Chen, J. L. Elkind, and P. B. Armentrout, J. Phys. Chem. **100**, 54 (1996).
[37] P. R. Kemper and M. T. Bowers, J. Phys. Chem. **95**, 5134 (1991); C. L. Haynes and P. B. Armentrout, Organometallics **13**, 3480 (1994).
[38] Y.-M. Chen and J. Armentrout, Chem. Phys. **103**, 618 (1995).
[39] Y.-M. Chen and P. B. Armentrout, J. Phys. Chem. **99**, 11424 (1995).
[40] D. Gerlich, Adv. Chem. Phys. **82**, 1 (1992).
[41] W. J. Chesnavich and M. T. Bowers, J. Phys. Chem. **83**, 900 (1979).
[42] N. Aristov and P. B. Armentrout, J. Am. Chem. Soc. **108**, 1806 (1986).
[43] R. H. Schultz, K. C. Crellin, and P. B. Armentrout, J. Am. Chem. Soc. **113**, 8590 (1991).
[44] P. B. Armentrout, in *Advances in Gas Phase Ion Chemistry*, edited by N. G. Adams and L. M. Babcock (JAI, Greenwich, 1992), Vol. 1, pp. 83–119.
[45] P. B. Armentrout, Int. J. Mass Spectrom. **200**, 219 (2000).
[46] G. Herzberg, *Molecular Spectra and Molecular Structure* (Van Nostrand Reinhold, New York, 1966), Vol. III.
[47] M. T. Rodgers, K. M. Ervin, and P. B. Armentrout, J. Chem. Phys. **106**, 4499 (1997).
[48] M. T. Rodgers and P. B. Armentrout, J. Chem. Phys. **109**, 1787 (1998).
[49] R. G. Gilbert and S. C. Smith, *Theory of Unimolecular and Recombination Reactions* (Blackwell Scientific, London, 1990).
[50] D. G. Truhlar, B. C. Garrett, and S. J. Klippenstein, J. Phys. Chem. **100**, 12771 (1996).
[51] K. A. Holbrook, M. J. Pilling, and S. H. Robertson, *Unimolecular Reactions*, 2nd ed. (Wiley, New York, 1996).
[52] M. J. Frisch, G. W. Trucks, H. B. Schlegel, *et al.*, GAUSSIAN 03, Revision B.02, Gaussian, Inc., Pittsburgh, PA, 2003.
[53] A. D. Becke, J. Chem. Phys. **98**, 5648 (1993).
[54] C. Lee, W. Yang, and R. G. Parr, Phys. Rev. B **37**, 785 (1988).
[55] K. Eichkorn, F. Weigend, O. Treutler, and R. Ahlrichs, Theor. Chem. Acc. **97**, 119 (1997).
[56] F. Weigend and R. Ahlrichs, Phys. Chem. Chem. Phys. **7**, 3297 (2005).
[57] D. Andrae, U. Haeussermann, M. Dolg, H. Stoll, and H. Preuss, Theor. Chim. Acta **77**, 123 (1990).
[58] D. Feller, J. Comput. Chem. **17**, 1571 (1996).
[59] K. L. Schuchardt, B. T. Didier, T. Elsethagen, L. Sun, V. Gurumoorthi, J. Chase, J. Li, and T. L. Windus, J. Chem. Inf. Model. **47**, 1045 (2007).
[60] J. Cizek, Adv. Chem. Phys. **14**, 35 (1969).
[61] G. D. I. Purvis and R. J. Bartlett, J. Chem. Phys. **76**, 1910 (1982).
[62] D. A. Prinslow and P. B. Armentrout, J. Chem. Phys. **94**, 3563 (1991).
[63] G. Kalus, U. Litzén, F. Launay, and W.-U. L. Tchang-Brillet, Phys. Scr. **65**, 46 (2002).
[64] W. C. Martin, R. Zalubas, and A. Musgrove, J. Phys. Chem. Ref. Data **19**, 821 (1990).
[65] K. Yoshizawa, Y. Shiota, and T. Yamabe, J. Chem. Phys. **111**, 538 (1999).
[66] G. Gioumousis and D. P. Stevenson, J. Chem. Phys. **29**, 294 (1958).
[67] T. M. Miller and B. Bederson, Adv. At. Mol. Phys. **13**, 1 (1978).
[68] S. G. Lias, NIST Chemistry WebBook, NIST Standard Reference Database No. 69, Eds. P.J. Linstrom and W.G. Mallard, National Institute of Standards and Technology, Gaithersburg MD, 20899, http://webbook.nist.gov, (retrieved June 24, 2009).
[69] H. P. Loock, L. M. Beaty, and B. Simard, Phys. Rev. A **59**, 873 (1999).
[70] S. F. Boys and R. Bernardi, Mol. Phys. **19**, 553 (1970).
[71] F. B. van Duijneveldt, J. G. C. M. van Duijneveldt de Rijdt, and J. H. van Lenthe, Chem. Rev. (Washington, D.C.) **94**, 1873 (1994).